ISOCAM PHOTOMETRY REPORT

Joris Blommaert

December 18, 1998

Version 2.1.1

1 Introduction

In this document a status report is given on the photometry of *point sources* with ISOCAM. An overview of the calibration stars and the stellar input models that have been used is given. The absolute calibration of the 2 detectors is discussed. Furthermore checks have been performed to see whether dependencies exist on different observing parameters like the integration time, the Pixel Field Of View, time in mission and orbit. Results of tests on the effect of transient correction on the photometry are described.

2 The calibration stars

Sixteen stars have been observed so far to calibrate the ISOCAM photometry (see Table 1). They were all selected from a list of calibration stars which were observed as part of the Ground Based Preparatory Programme (GBPP). Most stars are of early spectral type (A,F and G) but 3 K giants are also included. The flux densities at 4.5 and 12 μm are indicated and show quite a variety in flux levels (from 10mJy up to more than 10Jy). Because of the requested high visibility throughout the mission all sources are situated in a relatively small region of the sky which has an almost 100% ISO visibility (see Figure 1). In the selection of the stars it was also requested that the star was observed at least three times in the near-infrared in the GBPP. The stars were checked not to have any sign of variability nor to be part of a multiple system.

The visible magnitudes and the near-infrared photometry observed in the GBPP have been fitted with a Kurucz model by P. Hammersley (the data and the models can be found on the internal "Calibration Liaison web page": http://isou24.vilspa.esa.es:8888/) to provide the flux densities at longer wavelengths (see also several Calibration Working Group (CWG) meetings on this subject). The overall Spectral Energy Distribution is believed to be correct within 5%. Care has to be taken at some wavelengths where the stars may show spectral features, this is especially true for later type stars. Examples of

Table 1: Calibration stars used for photometry

HIC	HR	HD	RA (2000)	DEC (2000)	Spec Type	V (mag)	$F_{4.5}$ (Jy)	F_{12} (Jy)
065280		116405	13 22 45.13	+44 42 54.42	A0V	8.35	0.07	0.01
067485		120787	13 49 45.50	+61 29 21.30	G3V	5.97	5.3	0.9
069713	5350	125161	14 16 09.92	+51 22 02.17	A9V	4.80	3.5	0.5
070218			14 21 57.20	+29 37 46.47	K5V	8.56	1.1	0.2
070873	5423	127334	14 29 36.81	+41 47 45.41	G5V	6.38	2.0	0.3
073005		132142	14 55 11.08	+53 40 48.92	K1V	7.77	0.9	0.1
076568	5830	139798	15 38 16.22	+46 47 51.77	F2V	5.76	2.2	0.3
077277	5886	141653	15 46 39.99	+62 35 58.42	A2IV	5.19	1.6	0.3
077760	5914	142373	15 52 40.54	+42 27 05.64	F9V	4.62	10.1	1.6
085317		158485	17 26 04.86	+58 39 06.81	A4V	6.50	0.6	0.1
089474	6847	168009	18 15 32.47	+45 12 33.70	G2V	6.28	2.1	0.3
094890	7341	181597	19 18 37.84	+49 34 09.81	K1III	6.31	4.7	0.9
096062		184400	19 31 56.03	+48 35 34.59	F5	8.51	0.17	0.03
096441	7469	185395	19 36 26.50	+50 13 15.80	F4V	4.49	6.9	1.1
098962	7701	191277	20 05 32.85	+61 59 43.79	K3III	5.41	12.0	2.4
101245	7854	195820	20 31 21.17	+52 18 34.75	K0III	6.18	4.4	0.8

this are shown for the CO bands between 4 and 5 μm and the SiO fundamental around 8 μm (see Figure 2). The first plot shows a comparison of the Kurucz model with a more detailed model from B. Gustafsson (kindly provided by P. Morris, SIDT). The second plot gives a comparison of the Kurucz model with the "Cohen template" of γ Dra between 5 and 15 μm. The Kurucz model does not have any correction for the SiO fundamental. Basically there are ways to try to correct for the different spectral features (for instance by using the Cohen "composite spectra" (covering as much as possible in the 1 to 35 μm range from groundbased and KAO observations) and the "calibrated spectral templates", see for more information the Calibration Liaison web page), but the strategy we have chosen is to try to use early type stars and so keep corrections to a minimum. When this special care is taken we believe that this set of stars gives us the most reliable set of absolute flux calibrators.

3 Observations:

To determine the responsivity of the instrument the standard stars have been observed in all filters at least 6 times in the Performance Verification (PV) phase for LW and 4 times for SW. In Routine phase 10 times for LW and 7 times for SW. An overview of the observations is given in Table 2.

These observations are done in the following way. The source is observed at the centre of the array with 100 readouts of 2.1sec (1.5, 3 and 6$''$ PFOV are used, 1.5$''$ most frequently). For measurements made during the first part of the mission, the on-source observation is often followed by an Internal Calibration Device (ICD) measurement following the sequence designed for usage within the AOTs. For the longer wavelength filters (LW3, LW7, LW8, LW9 and LW10) also an off-source position is observed. For reasons of the transient correction (see later section on this subject) it was decided not to include the ICD-measurements any more and this was systematically done from Rev 384 onwards.

More stellar photometry measurements have been made to check possible dependencies of the point source photometry on Pixel Field Of View (PFOV) or integration time (see

Table 2: Overview of photometry on standard stars throughout the mission

Rev.	Target	Filters	lenses
30	73005	all LW	1.5
30	73005	LW1 LW6 LW9	3 6
34	70218	all LW	1.5
34	70218	LW1 LW6 LW9	3 6
34	70218	SW1 SW2 SW3 SW4 SW5 SW6	1.5
34	70218	SW3 SW4	3 6
38	70873	all SW	1.5
38	70873	SW3 SW4 SW5	3
38	70873	SW3 SW4	6
46	70873	all LW	1.5
46	70873	LW1 LW6 LW10	3
46	70873	LW4 LW6 LW10	6
58	77277	all LW	1.5
58	77277	LW1 LW6 LW10	3 6
58	77277	SW1 SW2 SW3 SW4 SW5 SW6	1.5
58	77277	SW3 SW4	3 6
62	85317	all LW	1.5
62	85317	LW1 LW6 LW10	3 6
62	85317	SW1 SW2 SW3 SW4 SW5 SW6	1.5
62	85317	SW3 SW4	3 6
66	73005	SW1 SW2 SW3 SW4 SW5 SW6	1.5
66	73005	SW3 SW4	3 6
78	85317	LW4 LW5 LW6 LW7 LW8 LW9 LW10	1.5
78	85317	LW1 LW6 LW10	3 6
100	77277	all LW	1.5
105	77277	SW1 SW2 SW3 SW4 SW5 SW6	1.5
112	77277	SW7 SW8 SW9 SW10 SW11	1.5
147	101245	LW3 LW5 LW6 LW7 LW8 LW9 LW10	1.5
154	101245	LW3 LW5 LW6 LW7 LW8 LW9 LW10	1.5
161	101245	LW1 LW2 LW4 LW10	1.5
161	101245	LW1	3
161	101245	LW4 LW6 LW10	6
161	101245	all SW	1.5
161	101245	SW3 SW4	3 6
196	101245	all LW	1.5
217	69713	LW3 LW5 LW7 LW8 LW9	1.5
237	77277	all SW	1.5
237	77277	SW3 SW4	3 6
265	98962	LW3 LW5 LW7 LW8 LW9	1.5
265	76568	LW1 LW2 LW4 LW6 LW10	1.5
279	77277	all SW	1.5
279	77277	SW3 SW4	3 6
314	98962	LW3 LW5 LW7 LW8 LW9	1.5
314	77277	LW1 LW2 LW4 LW6 LW10	1.5
314	77277	all SW	1.5
384	77277	LW1 LW6 LW10	1.5 3 6
384	98962	LW9	1.5 3 6
419	85317	LW1 LW2 LW4 LW6 LW7 LW10	6
419	85317	LW1 LW2 LW10	3
419	85317	SW1 SW4 SW5	1.5 3 6
419	89474	SW2 SW3 SW6 SW8 SW7 SW9 SW10 SW11	6
419	67485	LW3 LW5 LW8 LW9	6
419	67485	LW3	3
475	77760	SW8 SW9 SW10 SW11	1.5 3
552	65280	all LW	1.5
552	65280	LW3 LW5 LW8 LW9	3 6
552	77277	all LW	1.5
621	77769	SW7 SW8 SW9 SW10 SW11	1.5
621	89474	SW1 SW2 SW3 SW4 SW5 SW6 SW7 SW9	1.5
655	96062	LW3 LW9	1.5 3
846	96062	all LW	3
853	89474	all LW	1.5
867	85317	all LW	3,6
867	85317	LW1 LW6 LW10	12
867	89474	SW8 SW9 SW10 SW11	1.5
867	101245	SW1 SW2 SW3 SW4 SW5 SW6 SW7 SW9	1.5

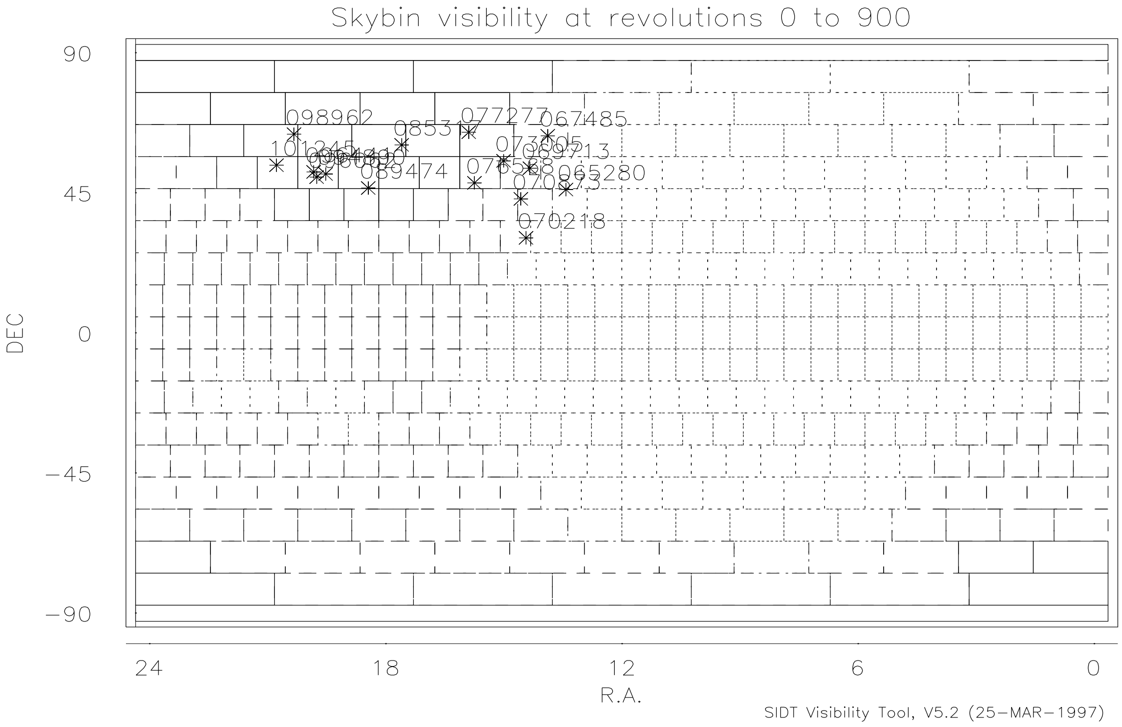

Figure 1: The ISO sky visibility. The selected calibration stars are in a region which has a high visibility throughout the mission.

Sections 7 and 8). Also HIC89474 has been observed regularly throughout the mission (see Section 9) to investigate the responsivity throughout the mission).

4 Data-Analysis:

All data-analysis was done within the CIA package. SPD data was taken from the archive and sliced into SCD's. The data was then analyzed in a standard way, meaning:

- Deglitching (method='temp')
- Scaled to gain 1
- On-board processing check
- Stabilised part estimation (method='Ksig')
- Average frames on the stabilised part
- Dark subtraction
- Detector flatfield correction
- Optical flatfield correction
- Background subtraction

Remarks:

– Deglitching: Several deglitching methods are available within CIA. With our observing method and for the bright sources we are using, the temporal deglitch turns out to be

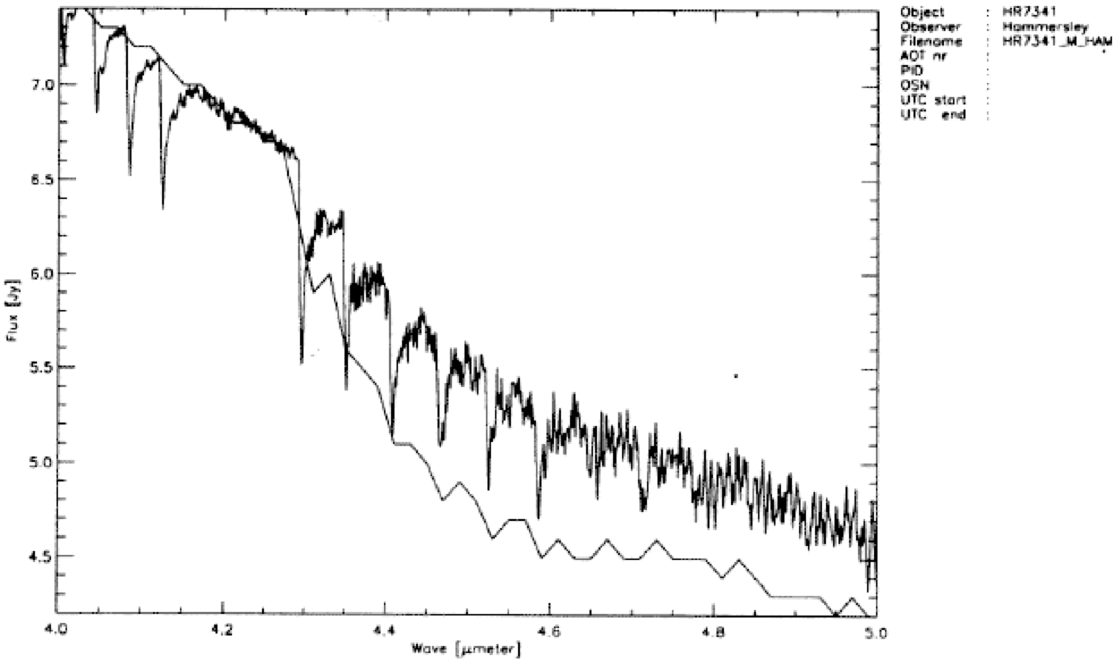

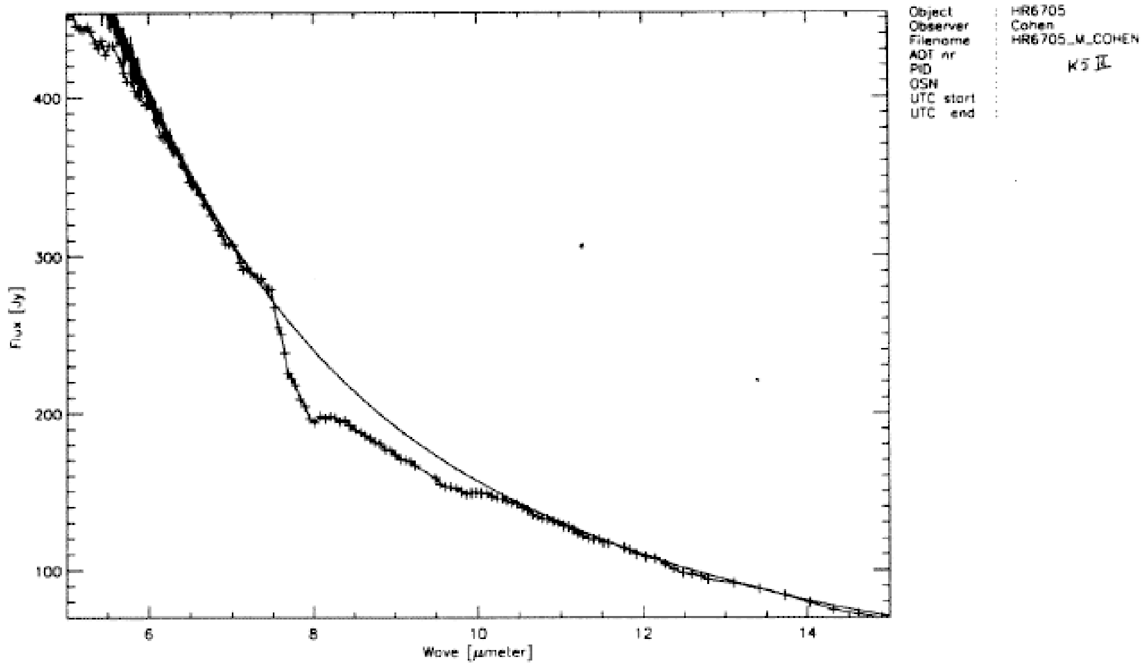

Figure 2: A comparison of the models used for the flux calibration around spectral features. The upper figure gives a comparison of the Kurucz model and a higher resolution model of the CO bands. Below the Kurucz model without correction for the SiO fundamental compared with the "Cohen template" of the same star.

the most stable one. Using 'MM' or 'TCOR' leads in some individual cases to a loss of about 25% in flux (this effect is caused by the fact that the deglitching routine, in combination with other routines 'masks' out bright pixels of the point source; see also the CAM Calibration Error Budget Report).
– Background subtraction: The background is subtracted by deriving the background from the edge of the image or by using a dedicated background. Up until revolution 384 the background measurement followed immediately the "on-source" measurement. This has as a result that in the "averaged" background image, often a trace of the source can be seen. By subtracting the on-source image with the background one the resultant flux is reduced by $\approx 3\%$. For this reason, unless the backgrounds were measured before the on-source measurements started, as done on rev 384 and later, no dedicated background was used in the analysis.
– Flux determination: Finally the point source flux is determined by using aperture-photometry and by scaling the resultant flux for the part of the PSF which was not included in the aperture. This factor was derived on a $1.5''$ pixelsize (256×256) image with a theoretical PSF. It was shown that the agreement of the observed PSF and the theoretical one is good (K. Okumura, ISOCAM PSF report). By taking such a big image it is possible to make comparisons for different lenses. The correction for the missing part of the PSF is an important one as the PSF's can be very large, especially at the longest wavelengths. For $1.5''$ and with an aperture of approximately 6 times the Airy disk ($\lambda(\mu m)/3$) the correction can be up to 20%.

5 The SENSITIV parameter:

The absolute calibration of ISOCAM is based on the stellar models of the GBPP (see section 2). The stellar models are believed to have an absolute accuracy better than 5%. The conversion of the measured signal in ADU/G/s to Jy is given by the SENSITIV parameter in the CCG*WSPEC files. The sensitiv parameter is given for the so-called reference wavelength. Until the OLP v5.0 the definition as used in the ISOCAM manual was followed (Tables 19 and 20 p. 87 and 88). During the mission it was decided to define a new set of reference wavelengths. The new reference wavelengths are "easy to remember" wavelengths and also give a better comparison with PHT and IRAS filters (see for further discussion the document in the Appendix: "Reference Wavelengths for ISO: CAM and PHOT filters; SAI/97-002/Dc, 17-Jan-1997). The new reference wavelengths are now used in OLP v6.0.

The procedure followed to derive the sensitiv parameter is the same as was adopted for IRAS. The convention used is that the conversion from measured signal (ADU/G/s) to Jy is given for a $\lambda F(\lambda) = const$ spectrum. As the spectral energy distribution of the input stars do not follow such a law (but rather $F(\lambda) \sim \lambda^{-4}$ a correction has to be applied (see following subsection)).

5.1 Colour correction

The SENSITIV parameter converts the ADU/G/s to fluxdensity in Jy for an input energy distribution which is constant in the logarithmic frequency interval ($F_\nu \sim \nu^{-1}$ or $F_\lambda \sim \lambda^{-1}$). When the observed source has an energy distribution different from the input one, a colour correction has to be applied.

In the CCG*WSPEC cal-G files the spectral transmission (Filter transmission $\times$ detector efficiency) for each filter is given. At this stage, no transmission curve for the lenses has been included.

$$R(\lambda) = FilterTransmission(\lambda) \times QuantumEfficiency(\lambda)$$

To determine the *actual* flux density one has to divide the flux density (derived after dividing the measured ADU/G/s by the SENSITIV parameter) by the colour correction factor.

$$F_{actual}(\lambda_{ref}) = F_{derived}/K(\lambda_{ref})$$

where $K(\lambda_{ref})$ is given by:

$$K(\lambda_{ref}) = \left(\int F(\lambda)/F(\lambda_{ref}) \times \lambda/\lambda_{ref} \times R(\lambda)d\lambda\right) / \left(\int R(\lambda)d\lambda\right)$$

5.2 The observed SENSITIV parameter

The LW detector

After the Performance Verification phase the photometric observations were analysed and compared to the "pre-launch" SENSITIV values. On average the point source photometry disagreed by about 25%. A modification was proposed where the SW SENSITIV values were multiplied by a factor of 1.2 and those of LW with 0.8. No filter to filter adjustments were made at that stage (ISOCAM Technical Note IAS-MP-960620). Furthermore a bug in the SW detector efficiency profile was overlooked so that the sensitivity quoted in the ISOCAM manual was underestimated for the shortest wavelengths. For these filters there was an additional correction of up to 1.5. These new values were included in the Cal-G CCG*WSPEC files used for OLP v.4.

For most LW observations done during PV and routine up to rev 265 the sensitiv parameter divided by the expected "pre-launch" value is given in Table 3. The in-flight sensitiv parameter has been derived by measuring the ADU/G/s and then dividing these by the colour-corrected (for a $F_\lambda = 1/\lambda$ spectrum) Jy's from the GBPP model of that star. Also indicated in this Table are the average and rms values of the sensitiv value for each filter. The spread in the sensitiv value 'Before rev389' is quite large for 2 reasons: i) the results used were derived at different stages during the mission using somewhat different routines, this lead to some changes in the derived values (eventually all photometry will be re-reduced with the present routines, but this has not been done so far) ii) the fact that no transient-correction has been applied and that the signals have not stabilised yet. The spread increases for longer wavelengths. In Figure 3 where the sensitiv parameter is

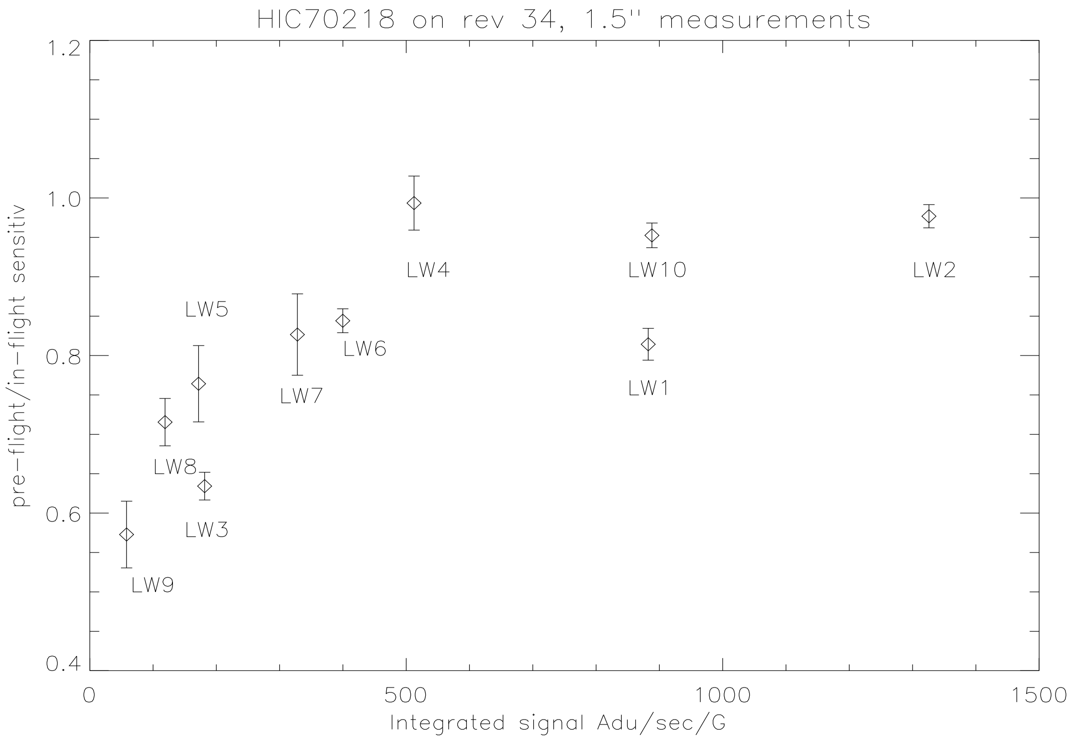

Figure 3: The LW SENSITIV values for hic 70218 (observed on rev 34) compared to the pre-launch values (note that the values given are in-flight divided by pre-flight, not as is stated at the y-axis). The deviations increase for decreasing flux levels.

Table 3: LW sensitiv values, comparison with ground-based

	'Before 384'				'Recent'			
Filter	N	Mean	RMS (%)	In-orbit / pre-launch	N	Mean	RMS (%)	In-orbit / pre-launch
LW1	12	0.72	6.7	0.79	10	0.78	4.1	0.86
LW2	5	1.93	6.2	0.88	7	2.30	3.3	1.05
LW3	7	1.34	17.	0.68	7	1.91	4.8	0.98
LW4	8	0.65	6.8	0.94	6	0.78	7.5	1.13
LW5	6	0.28	15.6	0.75	6	0.36	7.5	0.96
LW6	11	0.85	11.8	0.86	9	1.04	6.4	1.05
LW7	6	0.99	13.	0.78	9	1.33	6.7	1.06
LW8	6	0.49	17.	0.68	6	0.78	5.4	1.08
LW9	10	0.51	31.	0.67	9	0.64	2.8	0.85
LW10	8	3.32	10.	0.83	9	4.34	3.9	1.09

Table 4: LW sensitiv values, new wavelengths, colour corr. for A0V star

Filter	N	λ μm	Mean Adu/G/sec/mJy	RMS	col. corr.
LW1	12	4.5	0.77	0.04	1.02
LW2	5	6.7	2.32	0.08	1.08
LW3	7	14.3	1.96	0.09	1.03
LW4	8	6.0	0.78	0.06	1.02
LW5	6	6.8	0.35	0.03	1.01
LW6	11	7.7	1.03	0.07	1.00
LW7	6	9.6	1.33	0.09	1.01
LW8	6	11.3	0.78	0.04	1.00
LW9	10	14.9	0.65	0.02	1.01
LW10	8	12.0	4.23	0.23	1.29

shown for HIC70218 (rev 34) one can see that the deviations from the pre-launch values increase with decreasing flux levels. This is believed to be due to the fact that it takes longer for a signal to reach its final (stabilised) value when the ADU level is lower. A correction of this effect is discussed in Section 6.

In the following Figures (4-5) examples are given of how the signal is stabilizing throughout the measurement. The figures indicate the photometry of the source in each individual frame. This is done in a more crude way than on the final image but is just shown as an example of how the integrated flux is evolving. The large scatter is mostly caused by glitches which naturally affect photometry more on an individual frame than in the final averaged frame. It's clear that the observations in LW4 and LW6 have a more or less stabilised signal. This is not the case for LW10. For LW10 also an impression is given of how the background signal is evolving. The first plot shows that the signal is still decreasing at the end and has not or only barely reached its final value. The bottom figure of the dedicated background measurement in LW10 shows that now indeed a stable signal level has been reached. This is not the case in the top figure which shows the changing flux at the central position of the array (i.e. where the source was observed just before this dedicated background measurement). This still decreasing signal leads to a subtraction with a "too high" background level at the position of the point source. This leads to a 2 to 3% difference in the photometry with the case where the background is simply determined from the edges of the image.

Because of the stabilization problems a new observing strategy was used. No ICD measurements were included anymore. Also, the background measurements for all filters were observed before the source was observed. In a few revolutions 2 sources were used to observe all filters. In this way high signals could be reached for all filters (a star which doesn't saturate at the shortest LW wavelengths is relatively weak at the longest wavelengths). This change was included because the stabilization is slower for low flux levels and so in the earlier observations the longer wavelengths were not stabilized.

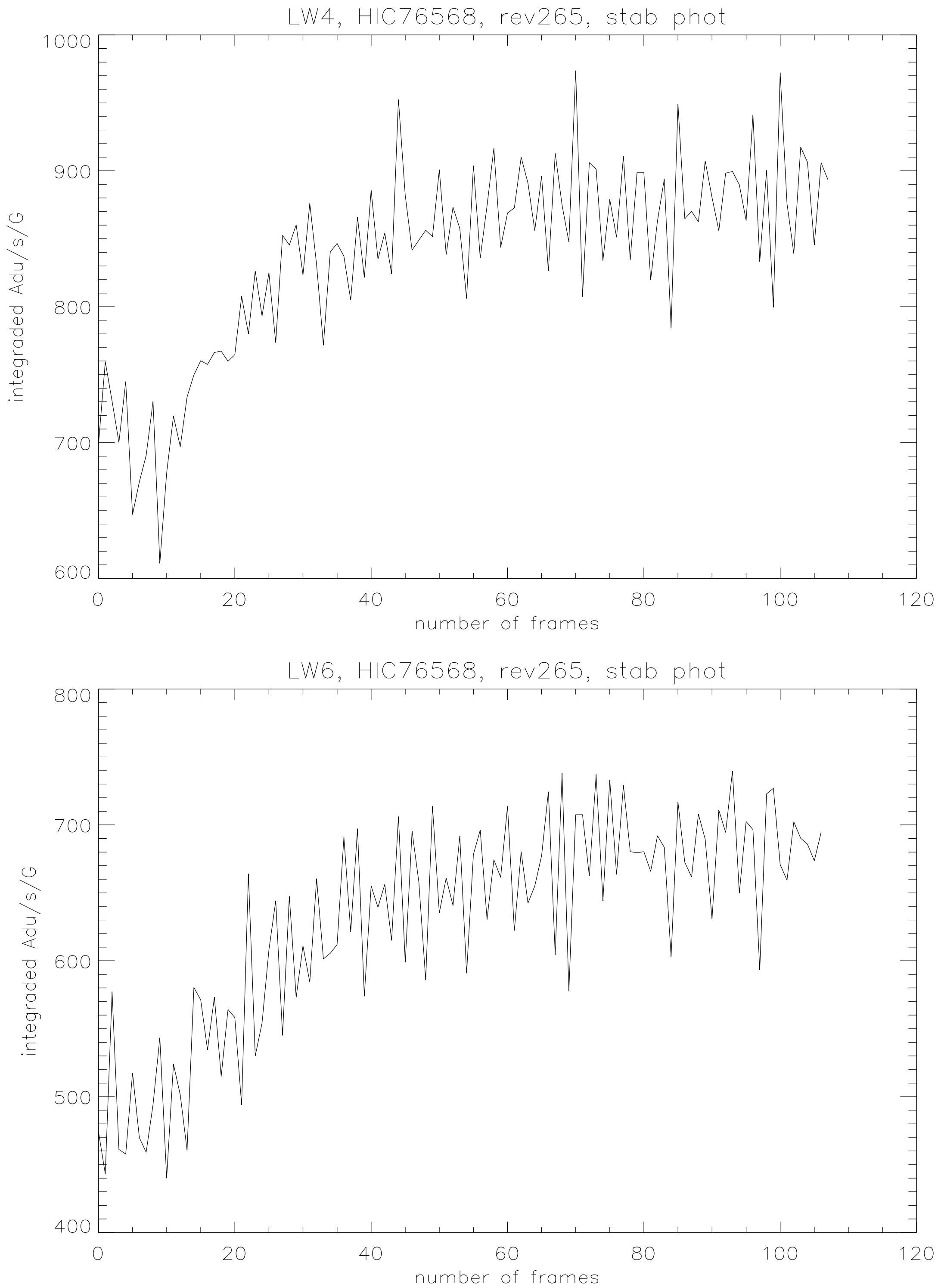

Figure 4: Examples of more or less stabilized signals. Photometry is performed on each individual readout.

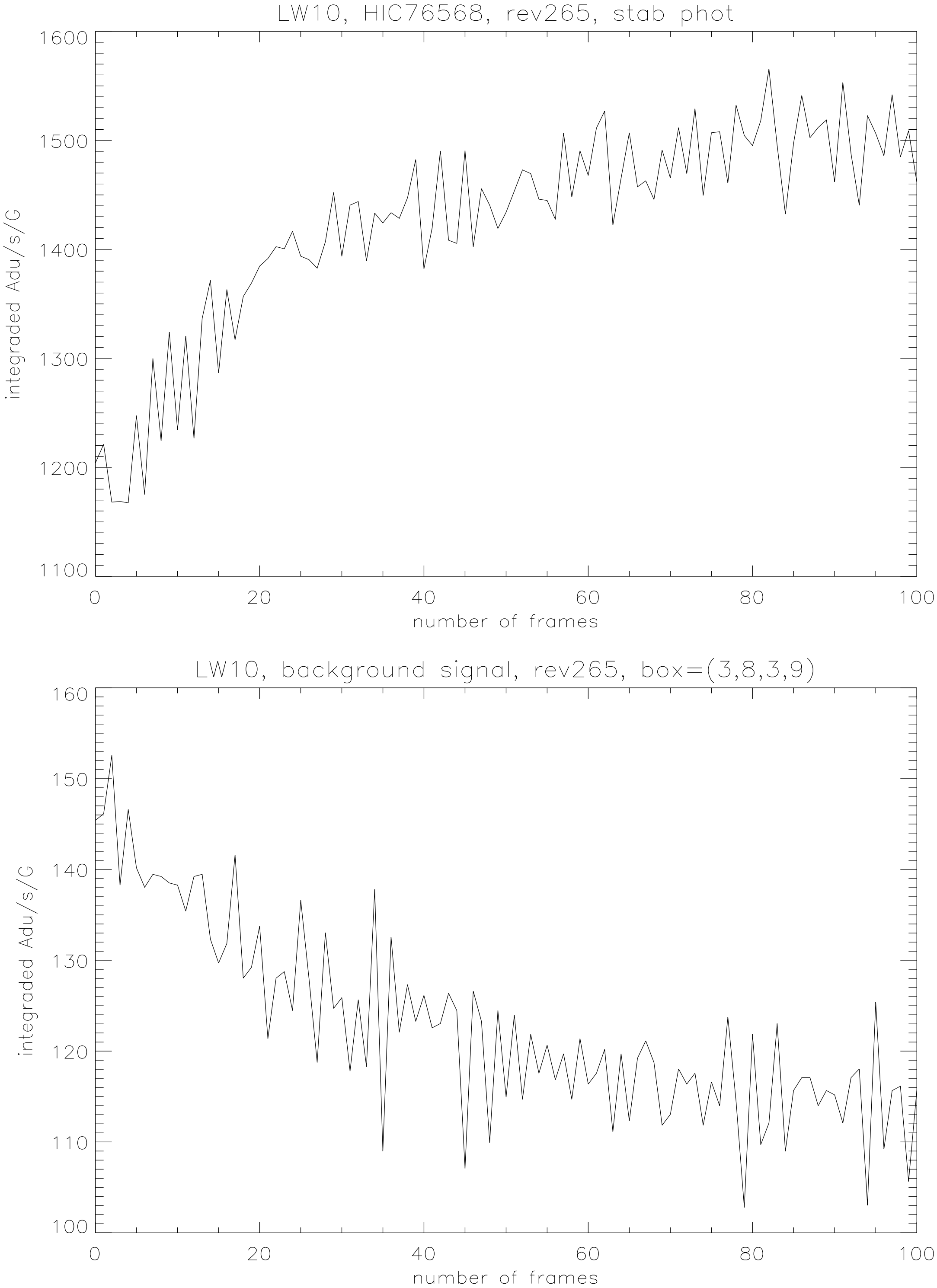

Figure 5: In the upper figure an example of a not-stabilized signal. Photometry is performed on each individual readout. In the lower panel one can see how the background signal is stabilizing (downward).

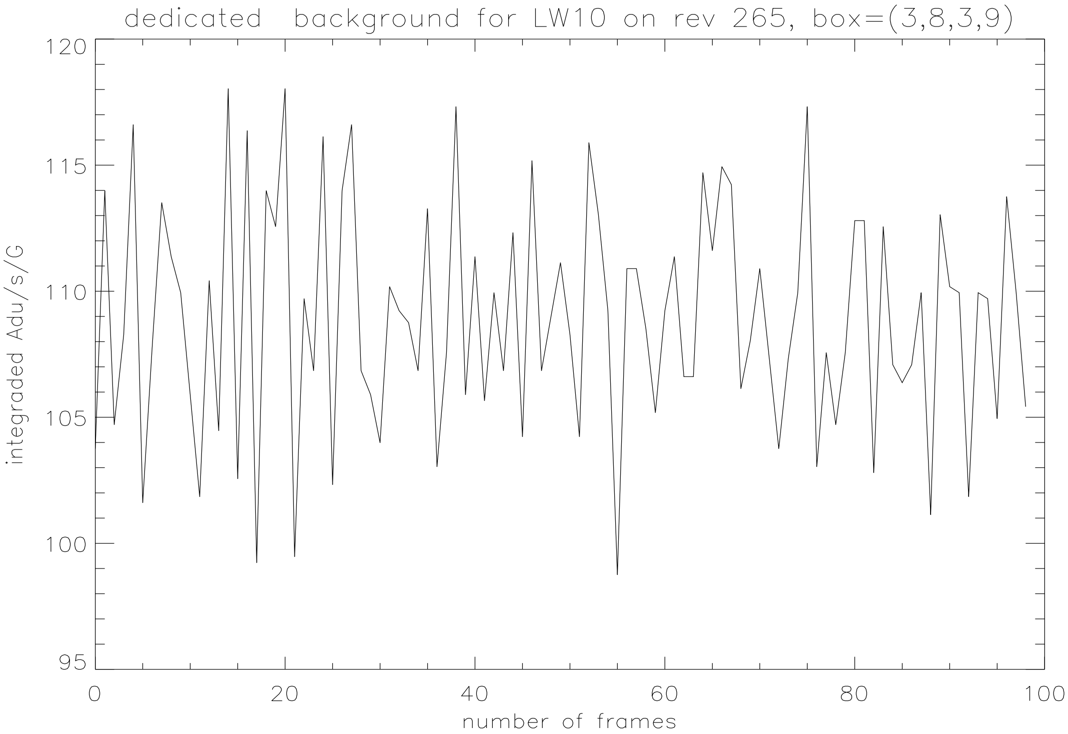

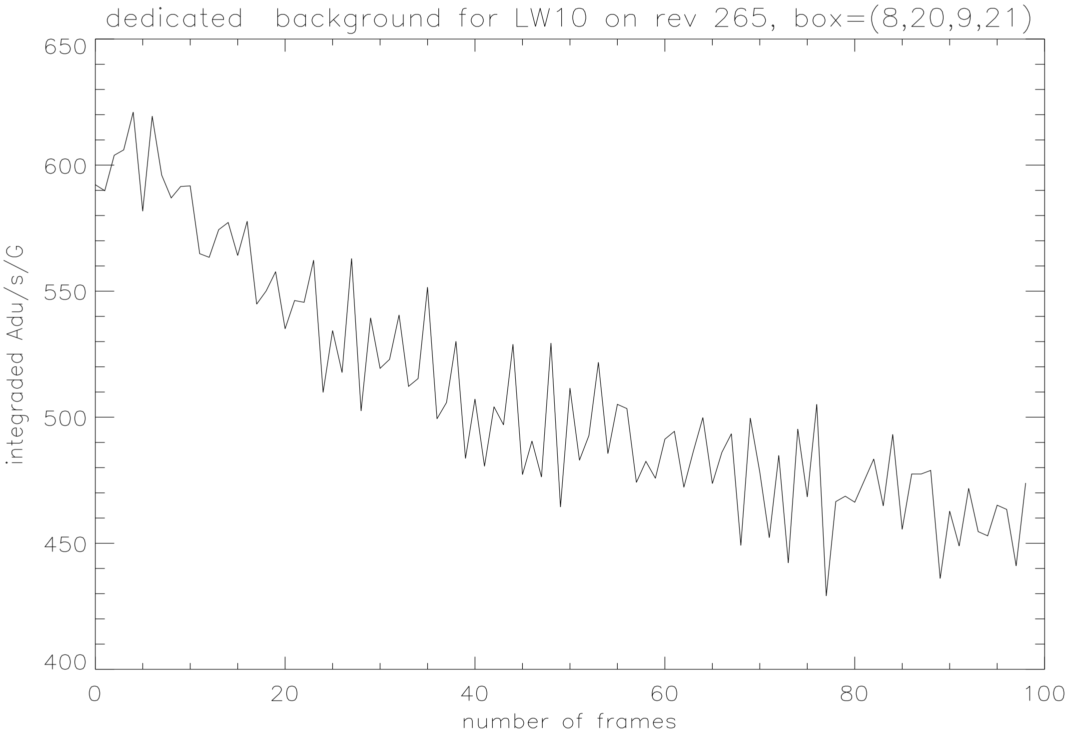

Figure 6: These plots show the signal evolution of the dedicated background measurement which followed the one in the previous figure. The lower plot shows the remnant of the on-source measurement. The upper plot shows that the background signal (away from the source) has stabilized.

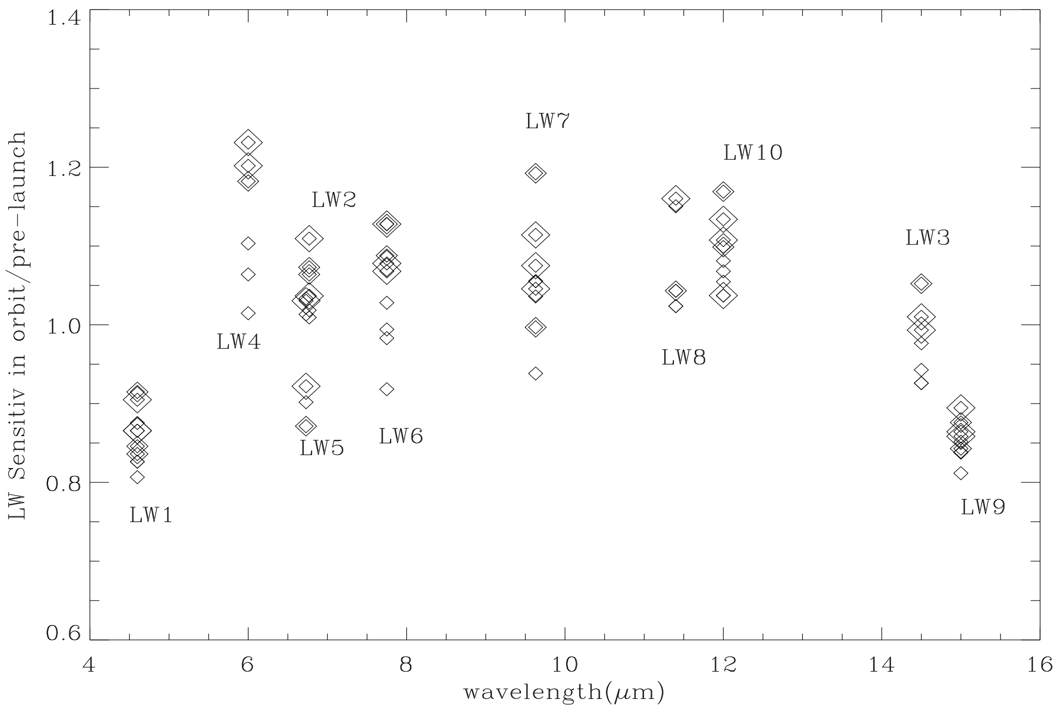

Figure 7: The in-orbit LW SENSITIV values compared to the pre-launch values. 1.5, 3 and 6″ PFOV measurements are included. The smallest symbols are 1.5″ and the largest are 6″ measurements.

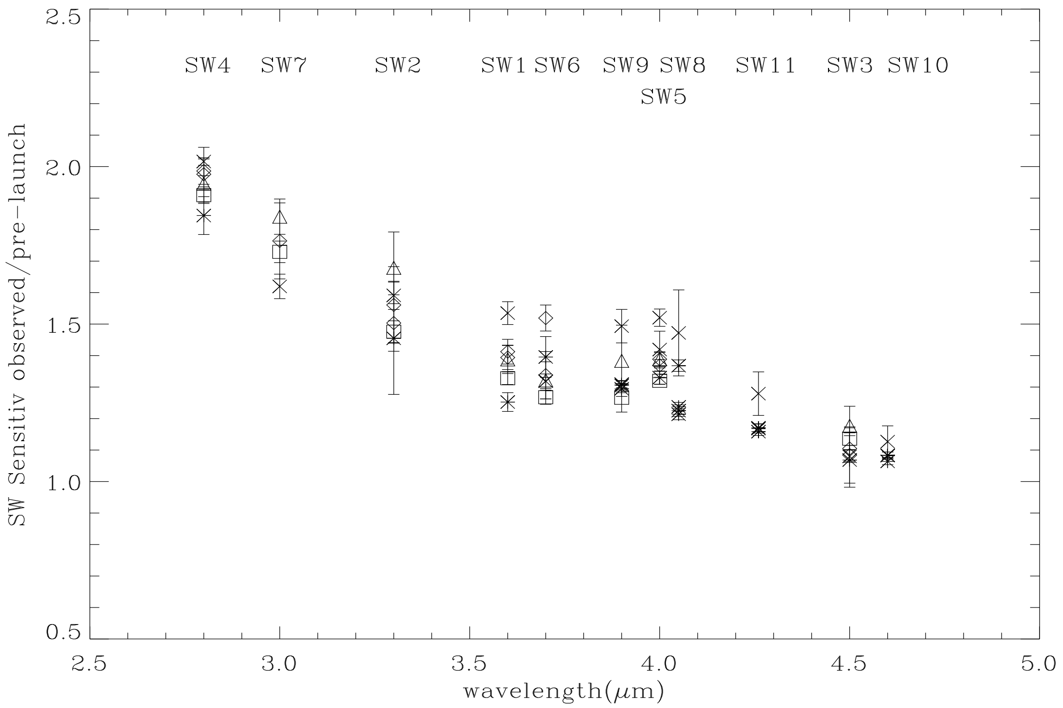

Figure 8: The in-orbit SW SENSITIV values compared to the pre-launch values. 1.5, 3 and 6″ PFOV measurements are included.

In Figure 7 and Table 3 the new results can be seen. It's clear that the LW in orbit/pre-launch values have increased and are closer to unity. This is caused by the new observing strategy where the fluxes in the different filters are better stabilized. Another difference is that now a correction is applied to include the point source flux that was not integrated by the aperture (see also the section on the data-analysis).

The spread around each filter measurement is smaller than in the 'older' results but is still larger than one would expect from the repeated measurements on HIC89474 (Section 8). This can be explained by the fact that different stars have been observed and so the uncertainties of the stellar models have to be included ($\sim 5\%$). Also stabilisation is still not completely reached in all cases. Especially the first filter measurement often has not reached a stabilised level (as an example: the LW7 filter measured at the start and the end of the HIC089474 observation gives 537.9 vs. 605.7 Adu/G/s). Another aspect that may enlarge the spread in the observed values is that no correction has been made for the change of the responsivity as function of time in the orbit (Section 9). A maximum difference between start and end of a revolution is about 5%.

As the reference wavelengths of the filters have slightly changed (see Appendix A) new sensitiv values and connected colour corrections are determined. In Table 4 the new sensitiv values can be found. The colour corrections given are those for a A0V star.

Table 5: SW sensitiv values

Filter	N	λ	Mean	RMS	col. corr.	In-orbit/pre-launch
		μm	Adu/G/sec/mJy	(%)		
SW1	8	3.6	0.41	4.6	1.05	1.41
SW2	6	3.3	0.12	4.9	1.04	1.56
SW3	6	4.5	0.26	3.4	1.06	1.11
SW4	6	2.8	0.30	2.9	1.02	1.97
SW5	8	4.0	0.77	4.8	1.04	1.39
SW6	5	3.7	0.19	6.0	1.01	1.31
SW7	4	3.0	0.16	4.5	0.96	1.76
SW8	6	4.05	0.038	7.2	1.02	1.29
SW9	5	3.9	0.074	5.8	1.03	1.31
SW10	5	4.6	0.092	2.5	0.98	1.08
SW11	5	4.26	0.058	5.5	1.02	1.17

The SW detector
For SW a re-analysis of the photometric observations was performed for the CAL-G delivery in January 1997 (used in OLP v6.0). The reason was that a new cross-talk correction was implemented. In Figure 8 the results can be seen. It's clear that in this version the values have gone up more than was proposed in the ISOCAM Technical Note IAS-MP-960620. In Table 5 the new values and their rms are indicated. The comparison with the ISOCAM 'pré-launch' and the in-orbit values is given (neglecting the difference between the new wavelengths and the ones in the ISOCAM manual, which gives only small differences on a percent level). For most filters the RMS is rather small (less than $\sim 5\%$).

There is a clear decrease in the difference with the groundbased sensitiv values and the ones observed in orbit with increasing wavelength. The reason is that in the routine determining the values given in the ISOCAM manual a 'λ-factor' was missing (private communication, M. Pérault). The ratio between the groundbased and in orbit sensitiv values for the SW filters is similar to the one found for the Spectral Response Functions measured pré-launch and in orbit (see the CVF report, Biviano et al).

6 Transient Correction

As the largest uncertainty in the photometry comes from the different stabilizations it was tried to correct for that by using a Transient Correction routine. The routine used is the so-called 'IAS'-model, which in CIA can be found under the program CORR_TRANSIENT_INV. The standard options of step=0.6 and a time constant = 1200 were used. Figure 9 gives an impression of the variations of the signal measured by the LW detector. The very high signal at the beginning comes from the ICD measurement, followed by a short period in which the instrument is reconfigured. From readout

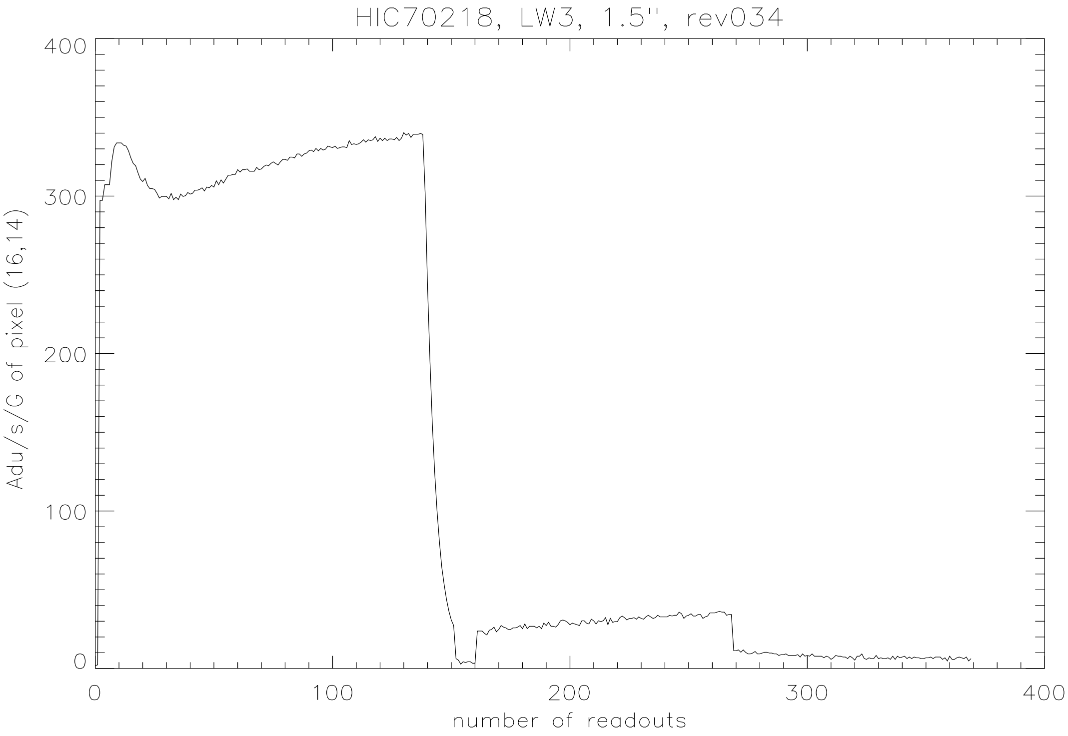

Figure 9: The history of the signal during the LW3 photometric measurement of HIC70218. The high signal comes from an ICD measurement, it is followed by an on-source and then a background measurement.

number 160 until 270 the observation is 'on-source' and then followed by an 'off-source' measurement. In the next Figure an example is given how the transient correction routine modifies the signal. In Figure 11 the photometric results are shown. Again the values are compared with the sensitiv values from the ISOCAM manual. Although these values are to be taken with some care (no colour correction (error of a few percent), nor a correction for the size of the PSF (up to 10%) has been included) it clearly shows that for the bright signals in the LW2, LW10, LW1 and to a lesser extent the LW4 no or only a small correction for the stabilization was performed. The weaker signals however are corrected and come much closer to the 'pre-launch' values. The odd point out is the LW3 which is only corrected for 20%. This result confirms that the largest uncertainty in the SENSITIV parameter is caused by stabilisation problems which hamper the weakest fluxes the most.

On a more recent revolution (621) HIC77277 was observed in all filters (without ICD). The same IAS transient correction routine was applied on this data. In Figure 12 the history of the signal and in a grey line the transient corrected one are shown. Only the first filter LW7 has a correction of about 10%. All the others have small corrections, less than 5%. This seems to indicate that by observing the source in the new strategy, even for lower flux levels, the source gets relatively well stabilized in each filter before the end of the 100 readouts measurement. In Figure 13 the results of REV 621 on HIC77277 are overplotted on the results of Figure 7. Most fluxes fall in the range of the already observed SENSITIV values. An exception is LW9 which has sensitiv value which is 10% higher

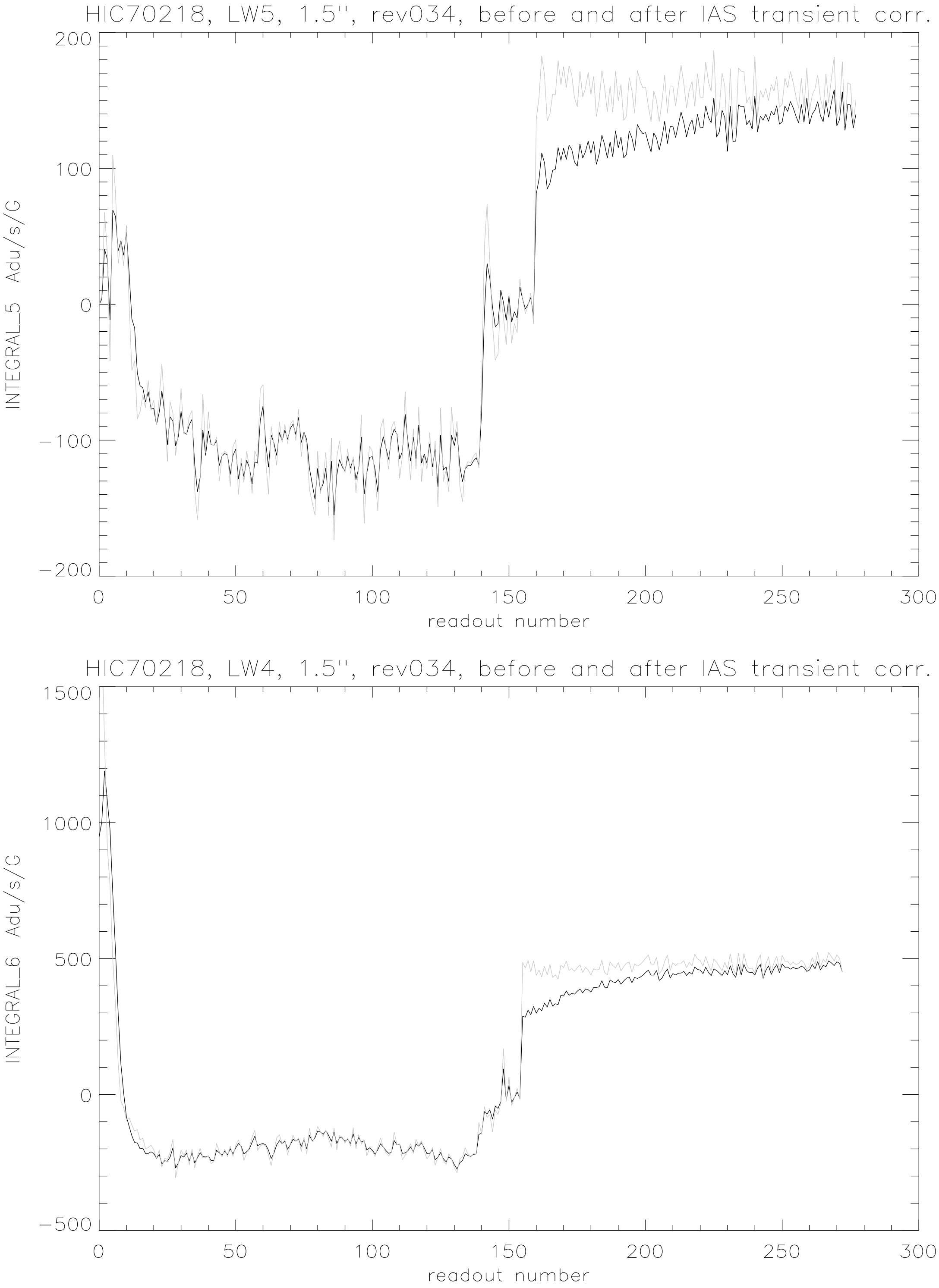

Figure 10: The history of the signal during the photometric measurement of HIC70218. The grey line is the transient corrected signal. The upper plot shows a clear change after TC, the lower one only gets corrected at the beginning of the on-source measurement.

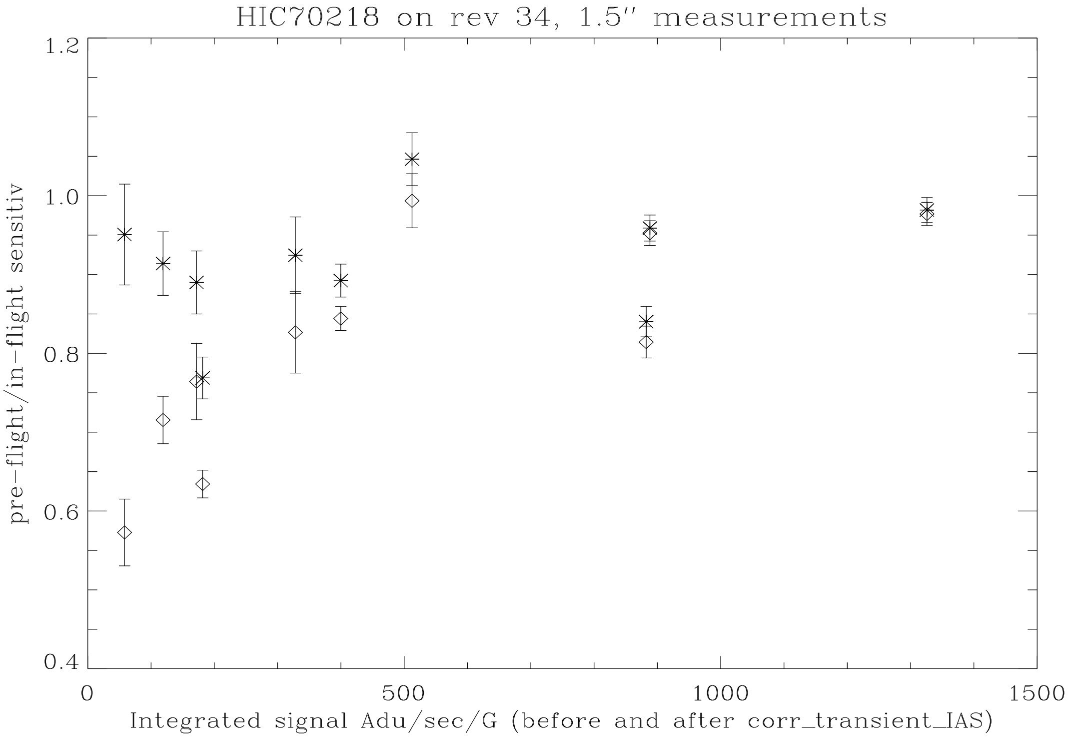

Figure 11: Same as Fig. 3, but now overplotted with transient corrected values: The LW SENSITIV values before (diamonds) and after TC IAS (asterisks). Again the y-axis should read in-flight divided by pre-flight.

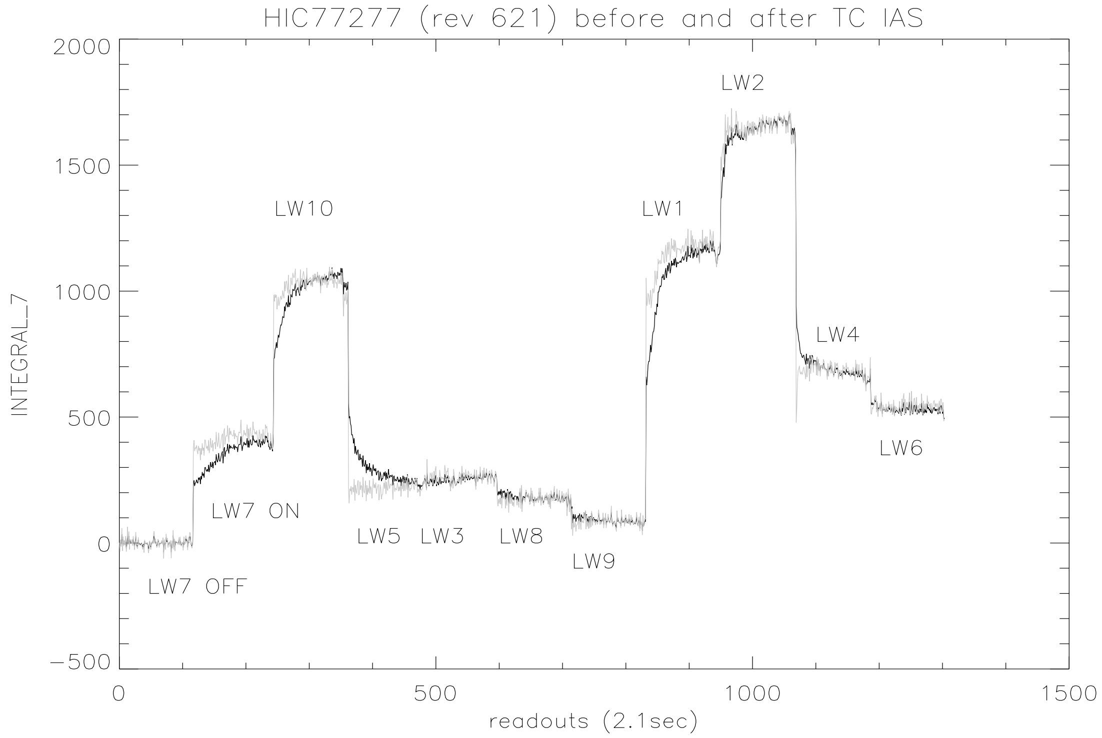

Figure 12: The history of the signal during the photometric measurement of HIC77277. The grey line is the transient corrected signal.

than all other LW9 measurements. Further analysis will have to explain the discrepancy.

6.1 HIC096062, a weak standard star

On Rev 655 HIC096062 was observed in the LW3 and LW9 filter, both in staring mode ($T_{int} = 5sec$, $N_{readout} = 100$) and in raster mode. The source is one of the faintest in the list of calibration stars ($F_{15\mu m} = 16.9mJy$) and was observed as a test of consistency between the normally bright standard stars and the often weaker "science" targets. As the source is relatively weak, the IAS method was applied to correct for the transient. The values given in Table 3 and this staring measurement agree very well: Adu/G/s/mJy value of 1.83 for LW3 (vs 1.91 in the Table) and 0.65 for LW9 (vs 0.64 in the Table) were found. For further investigation on faint sources and the comparison of the raster and staring observation see "The Faint Sources" document of B. Altieri.

7 Different T_{int}

On revolution 335 a calibration star was observed using different integration times. The measurements were done as follows: 750 seconds measurements done in the following sequence: .28, 2, 5 and 10, 5, 2, and .28 integration time. This strategy of a long measurement and repeating filters later on in the sequence was chosen as with earlier 'linearity' measurements (on Rev 58) the results were completely dominated by the differences in

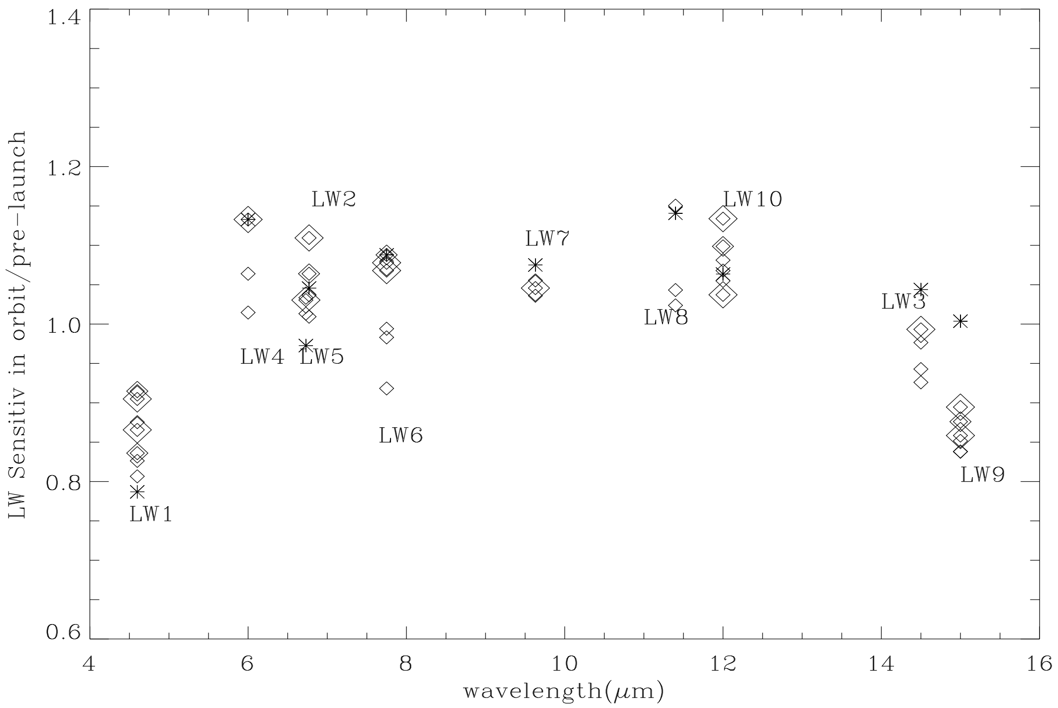

Figure 13: The comparison of the transient corrected (IAS) sensitiv value of HIC77277, rev621 (asterisk symbol) with the sensitiv values derived on the "brighter sources".

stabilization. The outcome of the Rev 335 observation is in Figure 14 and shows that no significant differences can be found between the different integration times (note that the first 2 sec measurement is still somewhat lower because of the still ongoing stabilization of the signal). The only possible difference is the 0.28 seconds integration time but that had to be redone as the S/N was too low.

On revolution 621 a new observation was scheduled so that now the 0.28 and 2.1 sec of integration could be significantly compared. The result is shown in Figure 15. There is still a somewhat upward trend in the photometry due to the continuing stabilization. But beyond that no difference is found between the two integration times.

8 Sensitiv and PFOV

From earlier results it was found that differences existed between the photometry performed with different lenses. As again differences in stabilization were possibly the cause of this, new measurements were planned in rev 384. The sources were observed at 6, 3 and 1.5″ subsequently with 300 readouts of 2.1 sec. The reduction was done as is described in section 4. Also all measured fluxes were corrected for the part of the PSF not included in the aperture. In Figure 16 the results are shown. Some differences are still found but they are small. There is some tendency that 1.5″ is somewhat weaker.

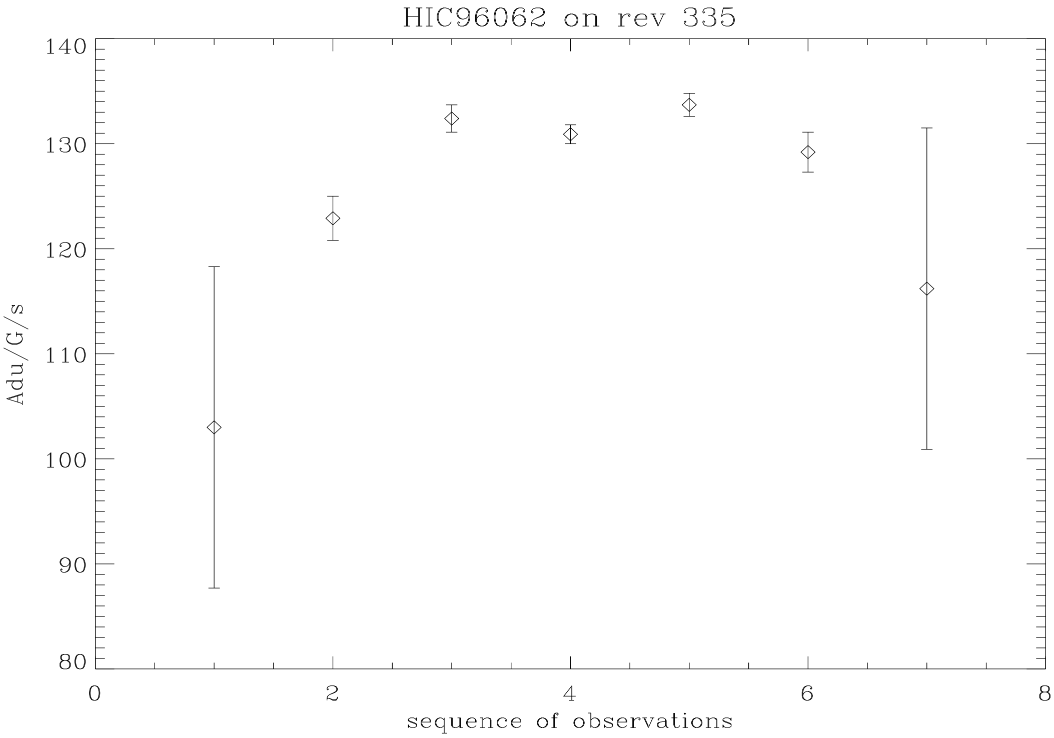

Figure 14: Comparison of the measured flux for different integration times. The sequence of observing is (from left to right in the plot) .28, 2, 5, 10, 5, 2, .28 sec.

9 Responsivity through orbit

HIC89474 (=HR6847) is regularly observed to monitor the responsivity throughout the mission. Filters used are LW2, LW10 and SW3. The source has also been observed to check the variation throughout the orbit. Figure 17 shows the LW2 photometry up to revolution 621. The difference between the maximum and minimum level is about 10% and the overall RMS is three percent. Figure 18 shows the variation of the responsivity as function of time since activation. There is a trend of decreasing responsivity with time since activation. By fitting a simple regression line to the data it is found that the response decreases along the following trend.

$$F(t) = F(0) - 8.3 \times t$$

A correction can now be made so that the photometry is scaled to the same time in orbit (here taken at mid-revolution). The photometry values in Figures 19 and 20 have been corrected for this. The correction has decreased the scatter in the observed values.

The same conclusions hold for the LW10 measurements (and the LW1 filter which was observed repeatedly on rev 349) so that we believe that this is a general trend in the LW behaviour.

SW also only shows a small variation throughout the mission (RMS= 2%) as can be seen in Figure 21 and no significant trend is found. In Figure 22 the observations are plotted as function of time in orbit. No significant trend is found.

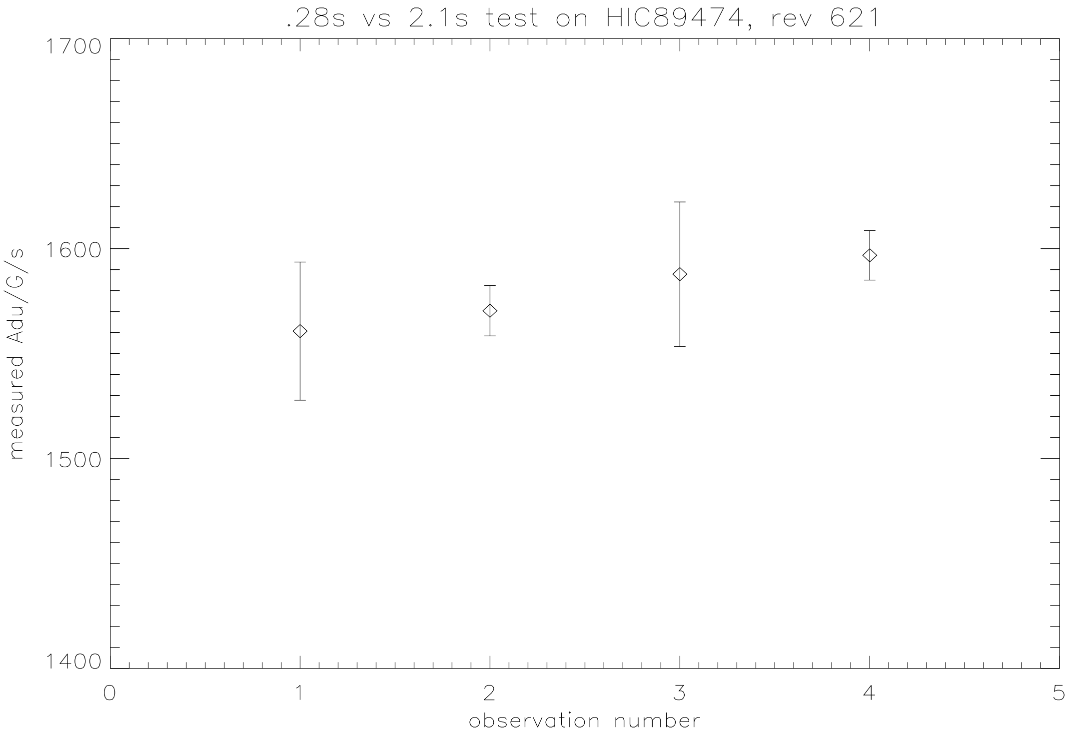

Figure 15: Comparison of the .28 and 2 sec integration time. Sequence is .28, 2, .28 and 2 sec.

The repeated SW observations on hic089474 show that there is a dependency on the source position at the array (Figure 23). The signal decreases by 3 to 4% when the source moves away by 5 pixels from the central pixel (in this case the source always moved mostly to the right on the array). The change in photometry is not caused by an increase in the background-value as we move closer to the border of the array. It is most likely a change in responsivity, although the image has been flatfielded.

10 Summary/Conclusions

The stars from the GBPP are a reliable set of objects which offer us the best possibility for an absolute calibration. Further measurements on red and weak sources were done to check the reliability of our responsivity values which are based on relatively bright sources.

The main problem in the photometry is the correction for the transient which means that especially filters where the flux is low have a larger scatter in the sensitiv value. For this reason, a new strategy of observing was adopted which is shown to be successful. We find that the responsivity is close to the pre-launch values for LW and about 50% higher for SW. Tests are performed to use the IAS transient correction model with preliminary results indicating that the photometry can indeed be improved. With better stabilized signals it is found that no or only small differences exist between different PFOV's.

The responsivity for LW decreases throughout the orbit with about 5% in total. No

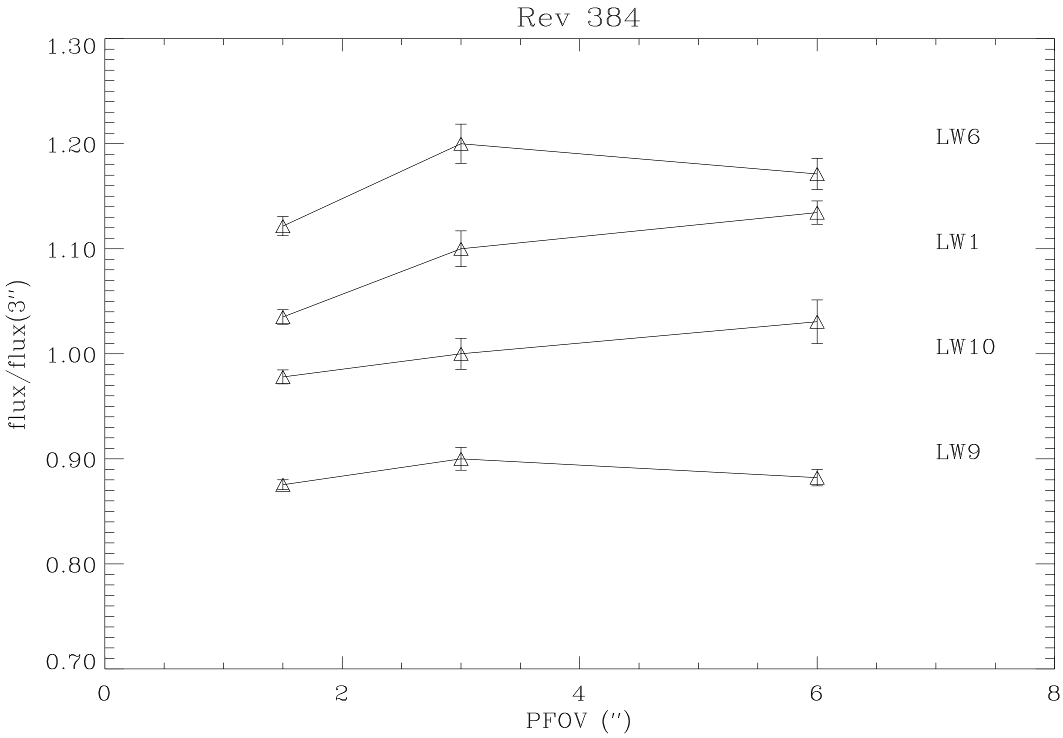

Figure 16: Comparison of the different PFOV. The fluxes are normalised to the flux at $3''$.

trend for LW or SW is seen throughout the mission.

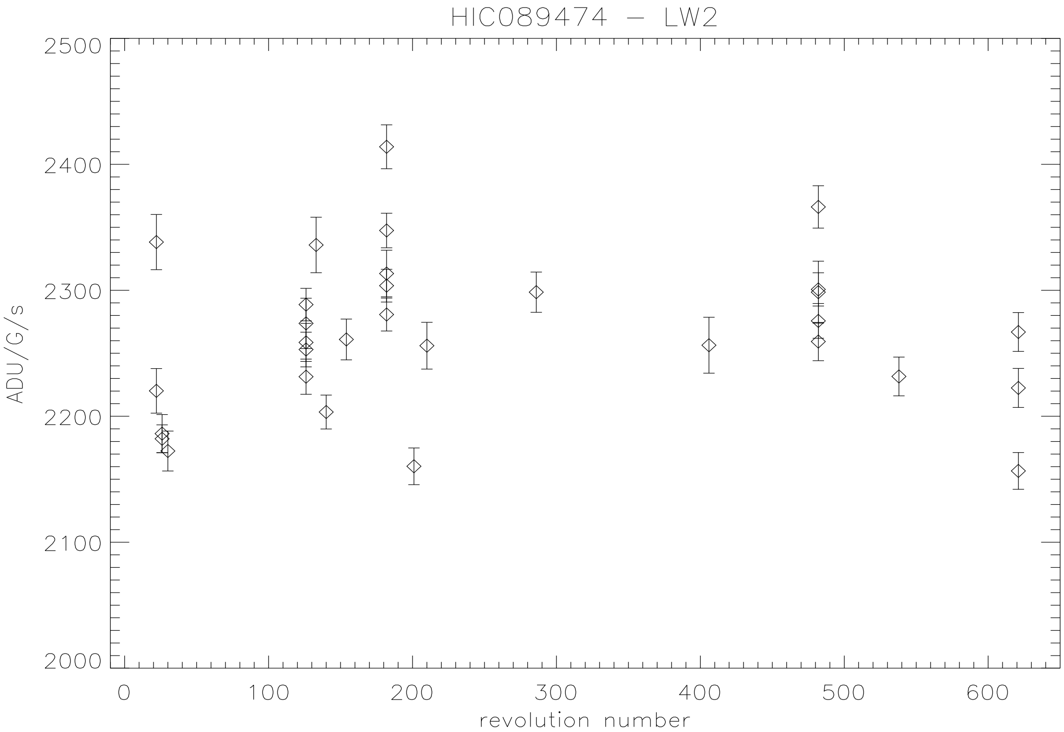

Figure 17: Photometry in the LW2 filter of HIC89474 throughout the mission as function of revolution number.

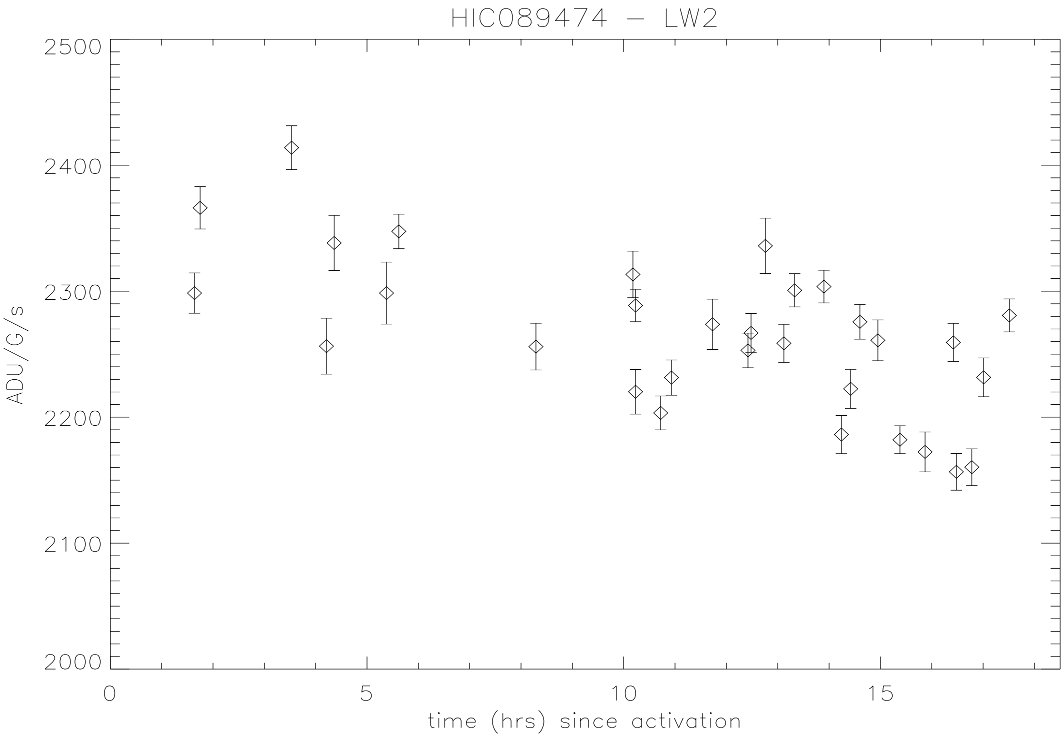

Figure 18: Photometry in the LW2 filter of HIC89474 throughout the mission as function of time since activation. There is a trend of decreasing responsivity throughout the orbit.

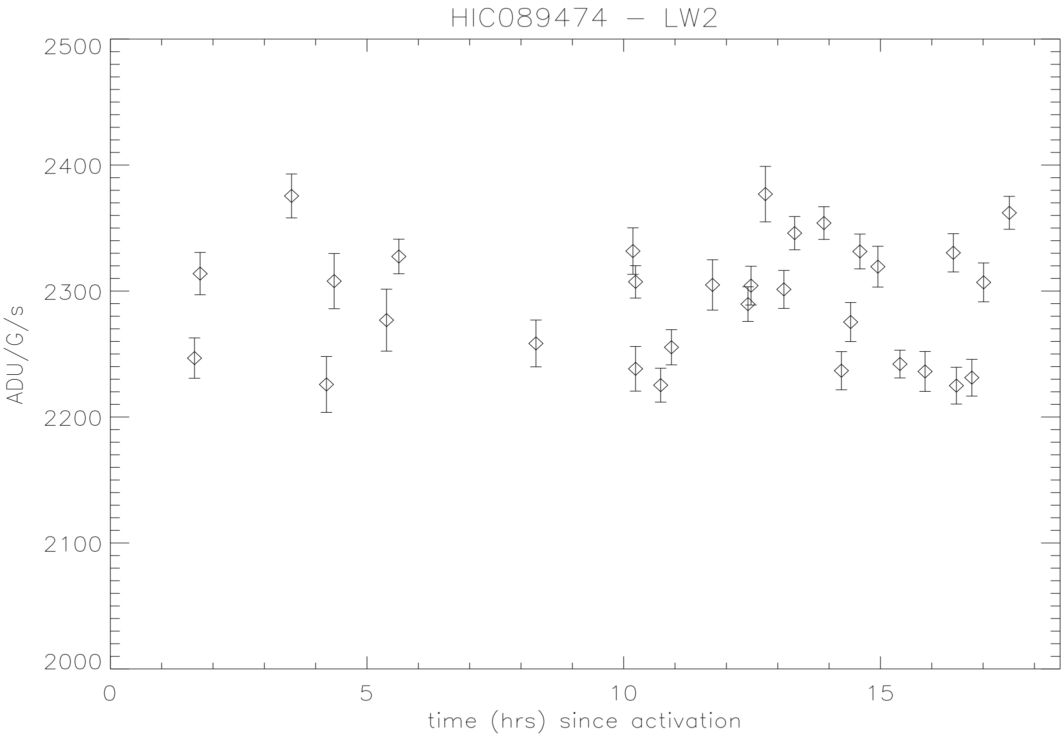

Figure 19: The photometry corrected for the trend through orbit.

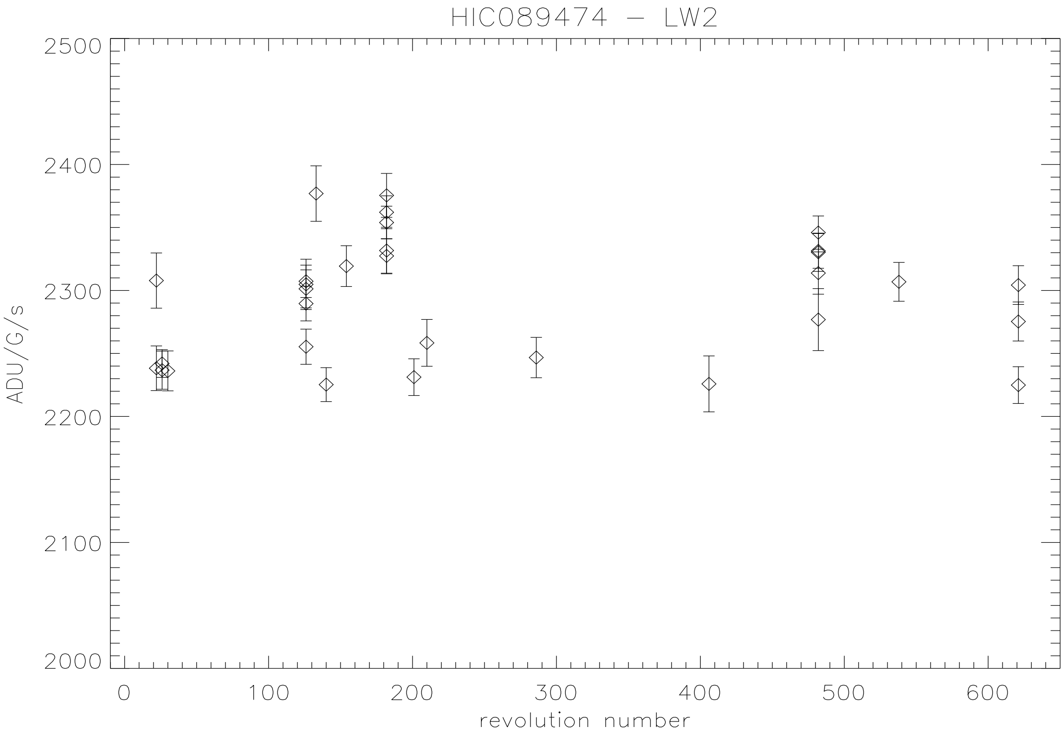

Figure 20: The photometry of HIC89474 corrected for the decreasing trend throughout the orbit.

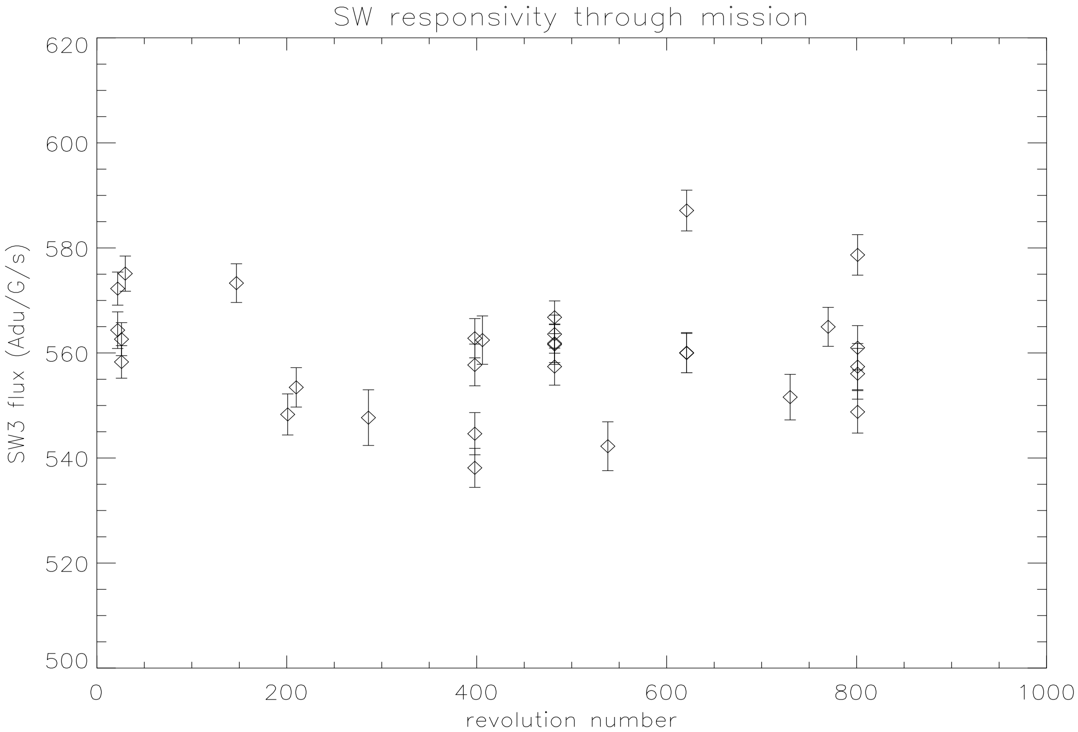

Figure 21: The SW3 photometry of HIC89474 throughout the mission.

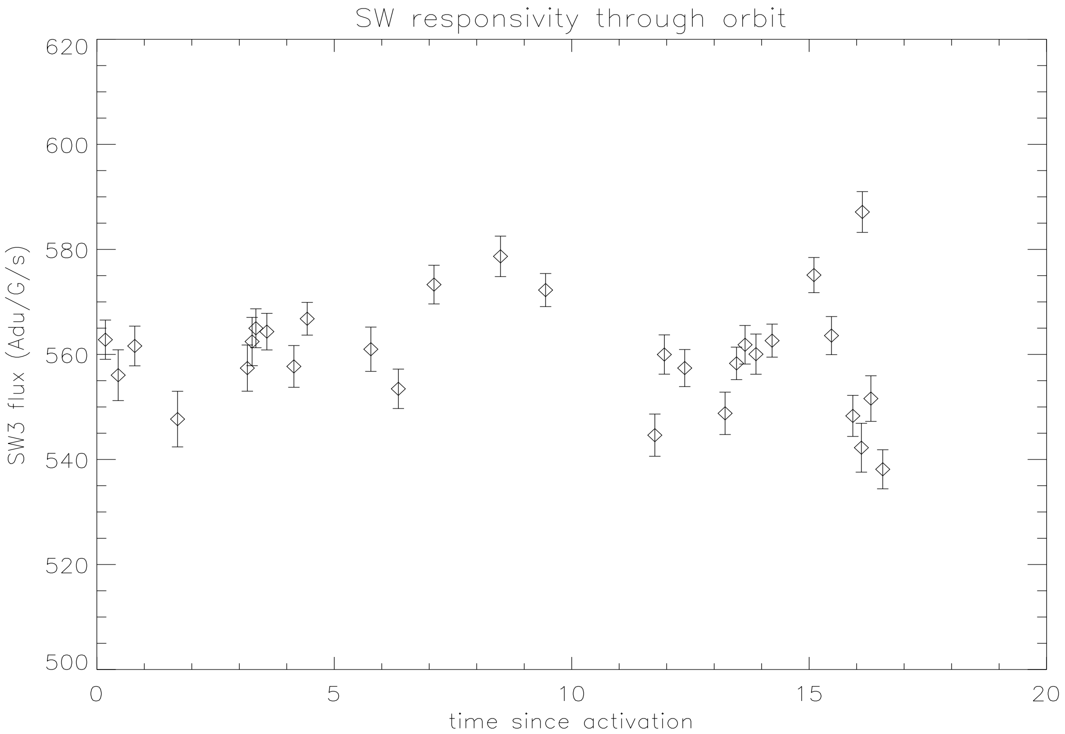

Figure 22: The SW3 photometry of HIC89474 throughout the orbit.

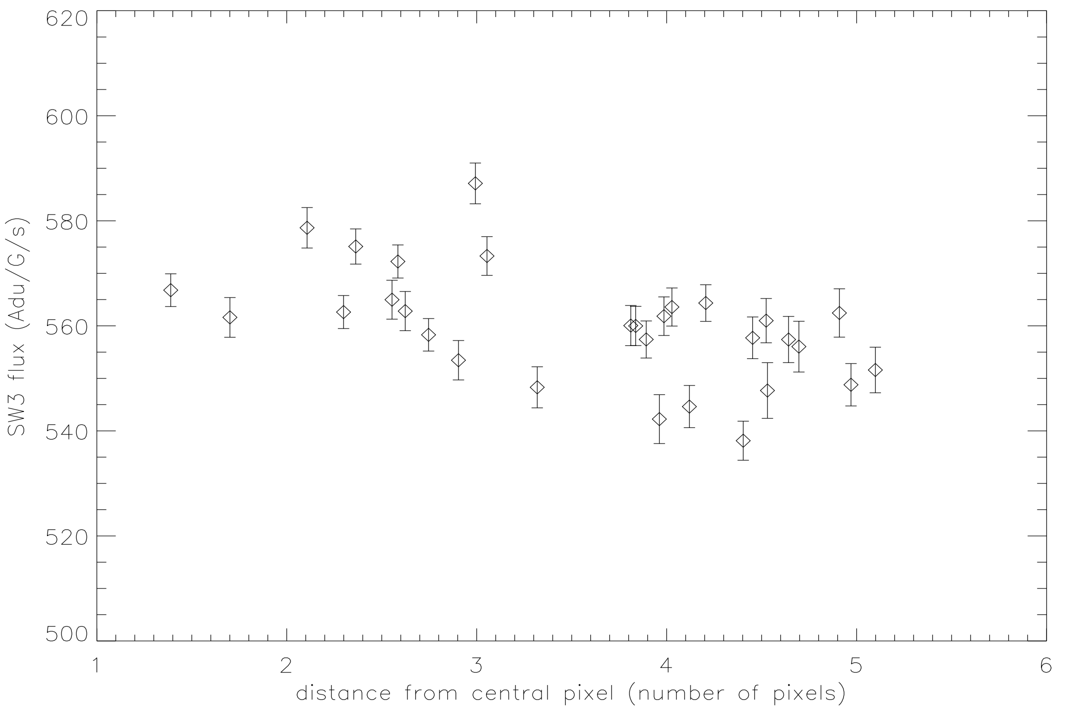

Figure 23: The SW3 photometry of HIC89474 as function of distance of the source to the central pixel of the array.

11 Appendix

Reference Wavelengths for ISO: CAM and PHOT Filters

Issue 1.0
SAI/97-002/Dc
17/Jan/97
Andrea Moneti, Leo Metcalfe, Bernhard Schulz

Reference Documents

R1)	ISO Reference wavelengths	SAI/96-240/Dc, 18/Dec/96
R2)	Golay 1974 in "Introduction to Astronomical Photometry", Ch. 2	

A1 Introduction

This document summarises discussions held over the last three months or so, for the most part in the context of the monthly Cross-Calibration meetings, on how to present ISO photometric measurements. Specifically, it will specify the manner in which in-band fluxes will be converted to monochromatic flux densities, and the choice of wavelengths to which these flux densities will be referred.

A2 Determining Flux Densities and Reference Wavelengths

The subject of the conversion of a heterochromatic photometric measurement to a monochromatic one has been summarised in R1, and full details can be found in R2. Following extensive discussion, the decision was made to adopt the IRAS convention, where the conversion is performed assuming a constant energy spectrum, i.e. $\lambda E(\lambda) = \nu E(\nu) = const.$ This has the advantage of making the results immediately comparable to IRAS data (though the filters are not identical), and the drawback that significant correction factors will have to be applied to most data, as was the case with the IRAS data, since most of the sources observed do not have a constant energy spectrum. These correction factors can be as large as $\sim 40\%$, and are largest for the broadest filters.

Alternative choices were:

1. to give only the in-band fluxes (in W/cm^2): these have the advantage of directly proportional to the what is measured and to be expressed in physical units, but since the depend of the filter bandwidth they cannot easily be compared to one another or to other data.

2. to give the ratio of the in-band flux of the source to that of a reference source expressed in magnitudes: these are awkward at best, mostly because they are not expressed in physical units. Furthermore, there is no single reference source that could span the complete ISO wavelength range.

3. to assume a model Sirius spectrum: this would produce correct results for nearly all normal stars, but incorrect results for peculiar stars, galaxies, and other objects. This is the scheme adopted by MSX, whose output catalog will consist primarily of stars (M. Cohen, private communication).

Options (1) and (2) would leave the conversion to monochromatic flux density entirely up to the user.

From the definition of isophotal wavelength, $\lambda_{\rm iso}$,

$$E \equiv \int_a^b E(\lambda)T(\lambda)\mathrm{d}\lambda = E(\lambda_{\rm iso})\int_a^b T(\lambda)\mathrm{d}\lambda, \tag{1}$$

where E is the measured in-band flux, and $T(\lambda)$ is the spectral response of the system, and with $E(\lambda) = 1/\lambda$, it follows that

$$E(\lambda_{\rm iso}) = \frac{E}{\int_a^b T(\lambda)\mathrm{d}\lambda}, \tag{2}$$

where the denominator is a property of the photometric system alone. And finally, to convert from $E(\lambda_{\rm iso})$ to $E(\lambda_{\rm ref})$ we use the relation

$$E(\lambda_{\rm ref}) = \frac{\lambda_{\rm iso}}{\lambda_{\rm ref}} E(\lambda_{\rm iso}). \tag{3}$$

Note that equations (2) and (3) define a linear relation between the in-band flux, E, and the flux density at the reference wavelength, $E(\lambda_{\rm ref})$.

From a formal point of view the choice of reference wavelengths is absolutely arbitrary. A reasonable choice of $\lambda_{\rm ref}$, however, will give *an idea* of the spectral energy distribution (SED) of the source, but in order to determine the true SED the user must convert $\lambda_{\rm ref}$ and $E(\lambda_{\rm ref})$ to $\lambda_{\rm iso}$ and $E(\lambda_{\rm iso})$ by using a known or assumed source spectral shape. For this purpose, "color correction tables" will be computed which will give correction factors and observed colours for many different types of energy distributions (namely power laws with different exponents, and Plank laws with a wide range of temperatures).

For the moment, and for the purpose of data presentation, a set of reference wavelengths has been chosen such that

1. they would clearly identify the filter, in particular where the filter is associated with a specific spectral band or line,

2. they are easy to remember numbers,

3. they are close to the $\lambda_{\rm iso}$ for either an $E(\lambda) = 1/\lambda$ spectrum or for Sirius.

The reference wavelengths that deviate the most from either isophotal wavelength are the ones for the IRAS filters, for which the IRAS wavelengths have been adopted. The reference wavelengths are tabulated in Tables 1 and 2 for CAM and PHT filters, respectively.

Table 6: CAM reference wavelengths

name	ref. λ	purpose	name	ref. λ	purpose
sw1	3.6	cosm.	lw1	4.5	Gen. Pur.
sw2	3.3	PAH	lw2	6.7	Gen. Pur.
sw3	4.5	Gen. Pur.	lw3	14.3	Gen. Pur.
sw4	2.8	Gen. Pur.	lw4	6.0	PAH
sw5	4.0	Gen. Pur.	lw5	6.8	Gen. Pur.
sw6	3.7	Gen. Pur.	lw6	7.7	PAH
sw7	3.0	Gen. Pur.	lw7	9.6	Silicates
sw8	4.05	Brα	lw8	11.3	PAH
sw9	3.9	Brα comp.	lw9	14.9	Gen. Pur.
sw10	4.6	CO fund.	lw10	12	IRAS
sw11	4.26	CO_2			

Table 7: PHT reference wavelengths

name	ref. λ	purpose	name	ref. λ	purpose
P3.29	3.3	PAH	C50	65	Gen. Pur.
P3.6	3.6	cosm.	C60	60	Gen. Pur.
P4.85	4.8	Gen. Pur.	C70	80	Gen. Pur.
P7.3	7.3	Gen. Pur.	C90	90	Gen. Pur.
P7.7	7.7	PAH	C100	100	Gen. Pur.
P10	10.0	Silicates	C105	105	Gen. Pur.
P11.3	11.3	PAH	C120	120	Gen. Pur.
P11.5	12	IRAS	C135	150	Gen. Pur.
P12.8	12.8	[NeII]	C160	170	Gen. Pur.
P16	15.0	Gen. Pur.	C180	180	Gen. Pur.
P20	20	Gen. Pur.	C200	200	Gen. Pur.
P25	25	IRAS			
P60	60	Gen. Pur.			
P100	100	Gen. Pur.			